Q. J. R. Meteorol. Soc. (1998), **124**, pp. 243–267

Secondary cyclogenesis: The initiation phase of a frontal wave observed over the eastern Atlantic

By HÉLÈNE RIVALS[1], JEAN-PIERRE CAMMAS[1]* and IAN A. RENFREW[2]
[1]*Laboratoire d'Aérologie, France*
[2]*University of Toronto, Canada*

(Received 25 September 1996; revised 4 June 1997)

SUMMARY

The initiation phase of a secondary frontal wave in the wake of a primary cyclogenesis event over the Atlantic is documented. North of the trailing surface cold front and south-west of the primary cyclone, an intense upper-level jet generates a direct and transverse ageostrophic circulation in its entrance region. Evidence is shown for two conflicting roles of this circulation: first, stabilization of the front through frontogenetic cross-frontal low-level convergence; and second, an increase of the potential for instability of the front through diabatic (e.g. latent-heat release) potential-vorticity (PV) redistribution in the upward branch of the circulation. Following saturation of the primary cyclogenesis and the associated along-front north-eastwards shift of the upper-level jet, the low-level branch of the ageostrophic circulation behaves like a zipper closing on the front, while in the upward branch an anomalous strip of PV builds along the cold front. Isentropic PV maps show that parcels of stratospheric origin embedded in the downward branch of the ageostrophic circulation (a tropopause fold) may have ended in the vicinity of the strip of anomalous low-level PV, perhaps contributing to an increase in the potential for instability of the surface front.

Using the domain-independent attribution method of Bishop, it is shown that the frontal wave forms on a part of the cold front where: first, the along-front stretching rate due to the environmental flow decays below the critical threshold value (0.6×10^{-5} s^{-1}) prescribed by theoretical studies; and second, the across-front frontogenetic component due to the ageostrophic circulation decays. This is consistent with semi-geostrophic theory, where the cross-frontal convergence and the stretching deformation are linked through the Sawyer–Eliassen equation. Results add to other recent observational findings: that the potential for instability, the evolving environmental flow and the induced ageostrophic convergence each have a crucial role in differentiating between frontal waves that will grow and those that will be suppressed.

KEYWORDS: Ageostrophic convergence Braer storm Frontogenesis Semi-geostrophic theory Stretching deformation

1. INTRODUCTION

Secondary frontal cyclones are sub-synoptic waves that develop along synoptic fronts embedded in mature large-scale extratropical cyclones. Over the North Atlantic such frontal waves develop in a preferential way, downstream and slightly south of the synoptic-scale storm track, according to a climatology of transient events based on a 10-year European Centre for Medium-Range Weather Forecasts (ECMWF) analysis database (Ayrault *et al.* 1995). Frontal waves hit the western coasts of Europe during 'zonal' weather regimes (Vautard *et al.* 1988). Most of them support only moderate signatures in surface pressure. However, they make a west European forecaster's work difficult as they are associated with precipitation and strong winds. A few frontal waves experience large and rapid deepening, like the Great Storm of October 1987 (Hoskins and Berrisford 1988; Jarraud *et al.* 1989). On the 1000 km horizontal scale, developmental processes of secondary frontal waves have recently experienced a remarkable renewal of interest; for example, Joly and Thorpe (1990); Schar and Davies (1990); Thorncroft and Hoskins (1990); Malardel *et al.* (1993); Bishop and Thorpe (1994a,b); Ayrault *et al.* (1995). This state of affairs has motivated scientists to propose international field campaigns to observe frontal waves over the Atlantic, e.g. the FRONTS 92 Experiment (Hewson 1993) and the Fronts and Atlantic Storm Tracks EXperiment (FASTEX) held in January and February 1997 (Joly *et al.* 1994, 1997).

The semi-geostrophic theory (Hoskins 1975) has provided theoreticians with a framework in which to investigate stability problems of fronts. A first group of studies (Joly

* Corresponding author: Laboratoire d'Aérologie, UMR CNRS/UPS 5560, Université Paul Sabatier, Toulouse, France.

and Thorpe 1990; Schar and Davies 1990; Malardel *et al.* 1993) undertook linear-stability analyses with a modal approach where the fronts satisfy the necessary condition for instability given by Charney and Stern (1962). Following Thorpe and Emanuel (1985), Joly and Thorpe (1990) hypothesize that latent-heat release provides the front with a potential for instability by producing an along-front extremum in potential vorticity (PV). This allows a barotropic or an internal baroclinic instability to take place. Theoretical results show that the most unstable normal modes grow with length-scales and time-scales typical of secondary frontal waves. However, even in the case of the nonlinear growth of normal modes (Malardel *et al.* 1993) wave deepenings were less than 10 hPa, hence the authors refer to these frontal waves as 'ordinary' frontal waves. For stronger frontal cyclones the necessity of a further baroclinic-instability phase of development, via either the ambient baroclinicity or an upper-level anomaly, has been put forward (Malardel *et al.* 1993).

Current progress with the stability analysis of fronts has been driven by the idea that the atmosphere responds very rapidly to particular initial conditions (Farrell 1984, 1989). Results using the adjoint technique (Joly 1995) confirm that larger mean-growth rates are reached when extracting from the basic frontal state the singular modes, rather than the normal modes. Results also suggest that non-modal frontal waves may develop even in stable fronts (in the sense of Charney and Stern) like the Hoskins-Bretherton (1972) pure-deformation front. Detailed observations of frontal waves throughout their life cycles are therefore necessary to show up underlying instabilities (Joly 1995).

A second group of theoretical studies (Dritschel *et al.* 1991; Joly and Thorpe 1991; Bishop and Thorpe 1994a,b) has involved fronts embedded in an evolving environmental flow. Numerical experiments allow horizontal shearing and horizontal deformation to be at work within time-dependent basic states. It was found (Joly and Thorpe 1991) that the action of horizontal across-front shearing does not directly impact on the frontal wave growth rate. A pure shearing deformation has no direct effect on the frontal wave properties, although indirectly a large horizontal cross-front shear will increase the potential for instability of a front. The measurements of cross-front shearing for several observed cases in Renfrew *et al.* (1997) indicate that it is not large enough to play an important role, when compared to the theory of Dritschel *et al.* (1991).

The parameter shown to be most important in theoretical models of frontal instabilities, with time-dependent basic states, is the along-front stretching deformation. Bishop and Thorpe (1994a,b) studied barotropic edge wave growth on an idealized moist tropospheric front in an external-deformation flow. They show evidence of two conflicting roles for the deformation flow and induced ageostrophic convergence. For strong along-front stretching the deformation flow will tend to inhibit all frontal wave development, by flattening perturbations along the front and pushing the growing waves out of the phase required for rapid growth. At the same time, via latent-heat release and diabatic redistribution of PV, the deformation flow and induced ageostrophic convergence will tend to increase the potential for instability of the front. If deformation ceases and the potential for instability is strong enough, then frontal waves will be free to develop along the front. A critical threshold value of the along-front stretching rate, γ_c, is proposed ($\gamma_c = 0.6 \times 10^{-5}$ s^{-1}). These theoretical considerations suggest that barotropic wave growth is likely to occur when strong along-front stretching is followed by a decrease in the along-front stretching. This is reminiscent of what occurs on the upstream tail of a long cold front, when the associated downstream main baroclinic system deepens and then becomes saturated.

Renfrew *et al.* (1997) applied the domain-independent vorticity and divergence method of Bishop (1996a,b) to four case studies of frontal waves observed over the Atlantic. The method allows an unambiguous association of flow fields, in a piece-wise manner, to vorticity and divergence elements inside a finite domain. Hence it provides a way of

partitioning the observed winds into a part due to any local structure, such as a front, and the remaining environmental flow. Diagnoses of wind derivatives, such as the horizontal deformation and frontogenesis, can then be performed on each part of the flow. Covering briefly four case studies, Renfrew *et al.* (1997) confirm the crucial roles of both the potential for instability and the evolving environmental flow in differentiating growth from suppression of frontal waves. Their results are broadly in line with the scenario suggested above, i.e. strong deformation decreasing over time to allow a wave to grow.

It is clear that detailed case-studies of frontal wave life cycles are also needed, especially in the context of preparatory work for FASTEX. The case-study chosen in this paper is the frontal cyclone that developed over the eastern Atlantic Ocean on 11–13 January 1993. It developed during a 'zonal' type regime (Vautard *et al.* 1988; Ayrault *et al.* 1995) and according to a subjective classification of frontal waves made by T. Hewson (Thorpe 1994) this case is a 'col' wave. The mature phase (12–13 January) of this cyclone as it moved over the United Kingdom has been studied by Browning and Roberts (1994). The mature phase of this cyclone also provides the test case for the PV retrodiction work of Fehlmann and Davies (1997). This paper is devoted to the initiation phase (11–12 January). Use is made of the T213/L31 ECMWF analyses, interpolated onto a polar stereographic conform grid (120 × 110 points, 75 km horizontal grid, 19 pressure levels ranging from 1000 hPa to 100 hPa).

In section 2 a synoptic analysis of the case-study is performed. ECMWF analyses are compared with some of the DMSP/SSMI* geophysical products, and the potential for instability of the initial cold front is characterized. Section 3 briefly presents the domain-independent attribution method (Bishop 1996a,b; Renfrew *et al.* 1997) and investigates the role of the large-scale deformation and local frontogenesis in the formation of the frontal cyclone. Section 4 synthesises the results in the framework of the life cycle of the frontal cyclone and presents conclusions.

2. Synoptic analysis

(*a*) *The parent low and the frontal wave*

The frontal cyclone chosen develops in the wake of a primary cyclogenesis event that broke the record for low pressure over the Atlantic (915 hPa; McCallum and Grahame 1993; Nielsen 1994), the so-called Braer storm. Figures 1(a) to 5(a) show the 24-hour evolution of the 1000 hPa geopotential height during the saturation phase of the Braer storm between Iceland and the north of Scotland. Associated with the surface trough, a trailing cold front extends across the Atlantic, as seen in the low-level gradient of equivalent potential temperature, θ_e (Figs. 1(b) to 5(b)). Note that the front is also fairly well defined in gradients of potential temperature, θ (see Fig. 8), any frontolytic sea surface heat fluxes do not appear to be having much effect in this particular case.

The frontal wave develops in the col pressure area between two anticyclones over Canada and the Azores. The key date of the frontal wave formation was taken to correspond with the first ECMWF analysis showing a closed 1000 hPa isohypse along the low-level trough. According to this criterion, the frontal wave forms at 38°N 38°W around 1800 UTC 11 January 1993 (Fig. 3(b)). This criterion could be relevant only for this case-study, as one can of course produce closed isohypses simply by changing contour interval. However further results using the 'frontal waviness', a measure of the frontal wave growth defined by Renfrew *et al.* (1997), will confirm this key date. Later on (Figs. 4 and 5) the wavy shape of the cold front develops and the positive equivalent-potential-temperature anomaly

* Defense Meteorological Satellite Program/Special Sensor Microwave Imager.

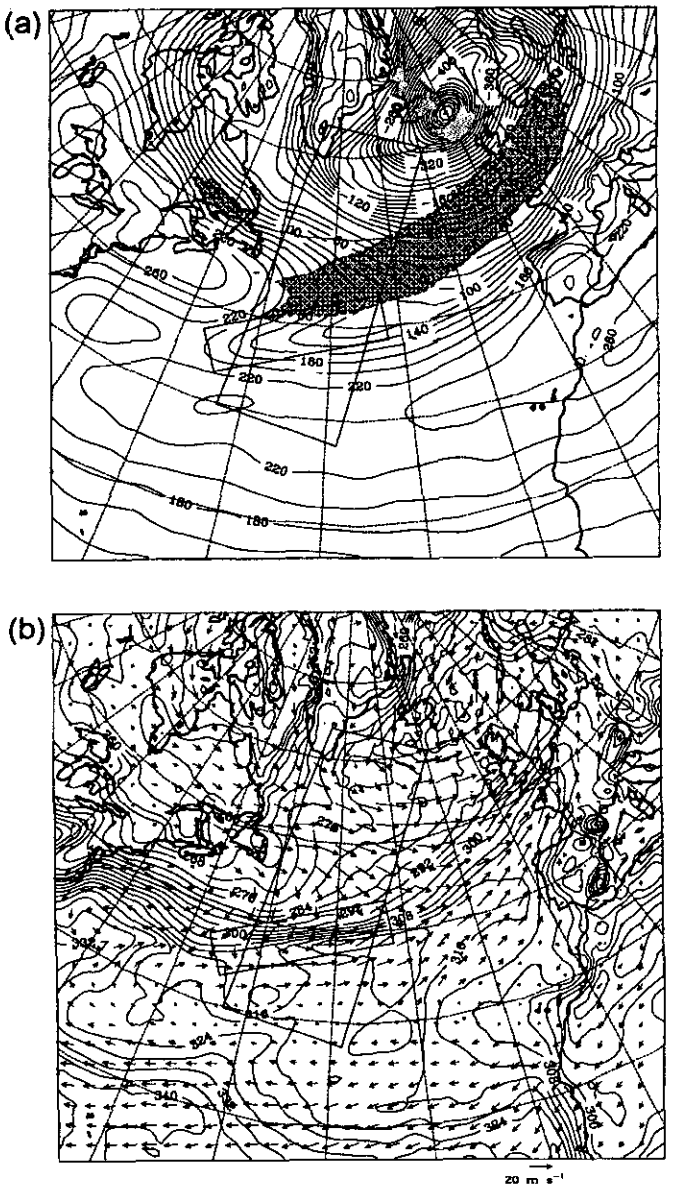

Figure 1. Analysis at 0600 UTC 11 January 1993: (a) 1000 hPa geopotential height (solid lines, contour interval 20 m), and where the 300 hPa wind speed exceeds 60 m s^{-1} (dark shading); frontal box B1 is also shown. (b) 1000 hPa equivalent potential temperature (solid lines, contour interval 4 K), and 1000 hPa wind vectors (a reference vector is given near the lower right-hand corner); frontal box B2 is also shown. The path of the DMSP/SSMI orbit at 0830 UTC 11 January 1993 is given in both (a) and (b). See text for further explanation.

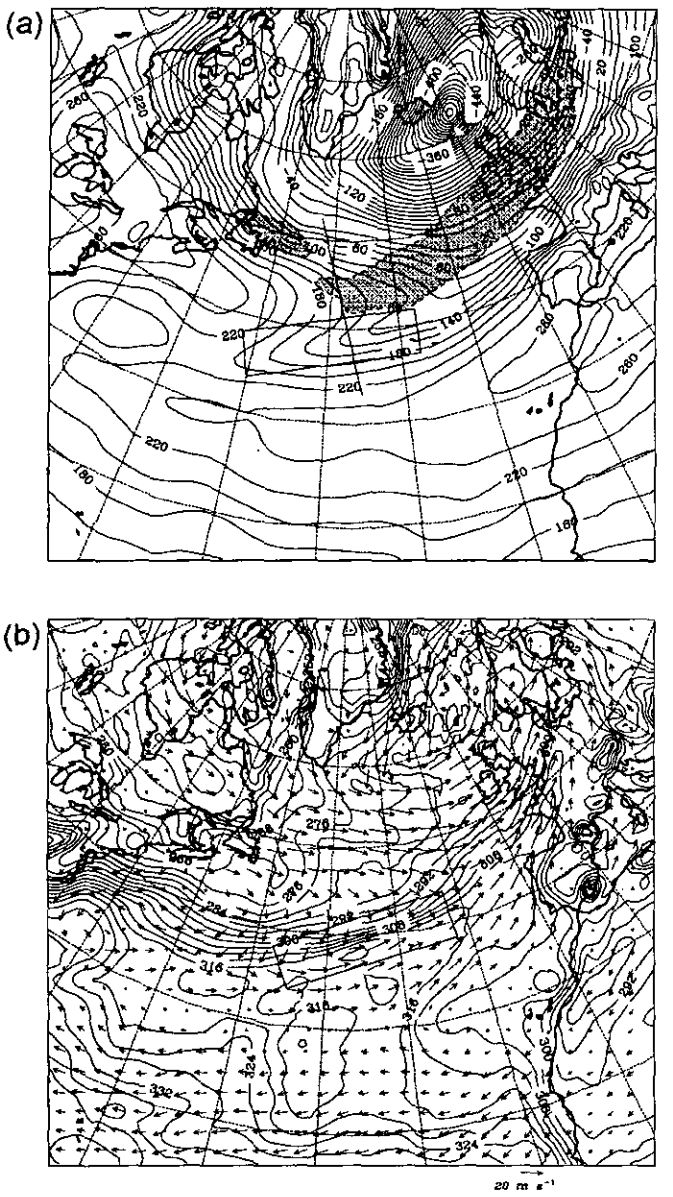

Figure 2. Analysis at 1200 UTC 11 January 1993, as Fig. 1. The location of the vertical cross-section shown in Figs. 7(a) to 7(d) is marked in Fig. 2(a).

increases. Satellite images confirm the wavy behaviour of the front as seen on total water vapour content fields from the two DMSP/SSMI passes (Figs. 6(a) and (b)). The first pass (Fig. 6(a)) spans the cold front west of the Azores at 0814 UTC, about 10 hours before the event. The second pass spans the western half-wavelength of the incipient frontal cyclone in the same region a day later (0827 UTC, 12 January). A very good agreement is found with the position of the front in the ECMWF analyses. The width of the strip of maximum water vapour content is about 300–350 km. The latent heat released by the condensation

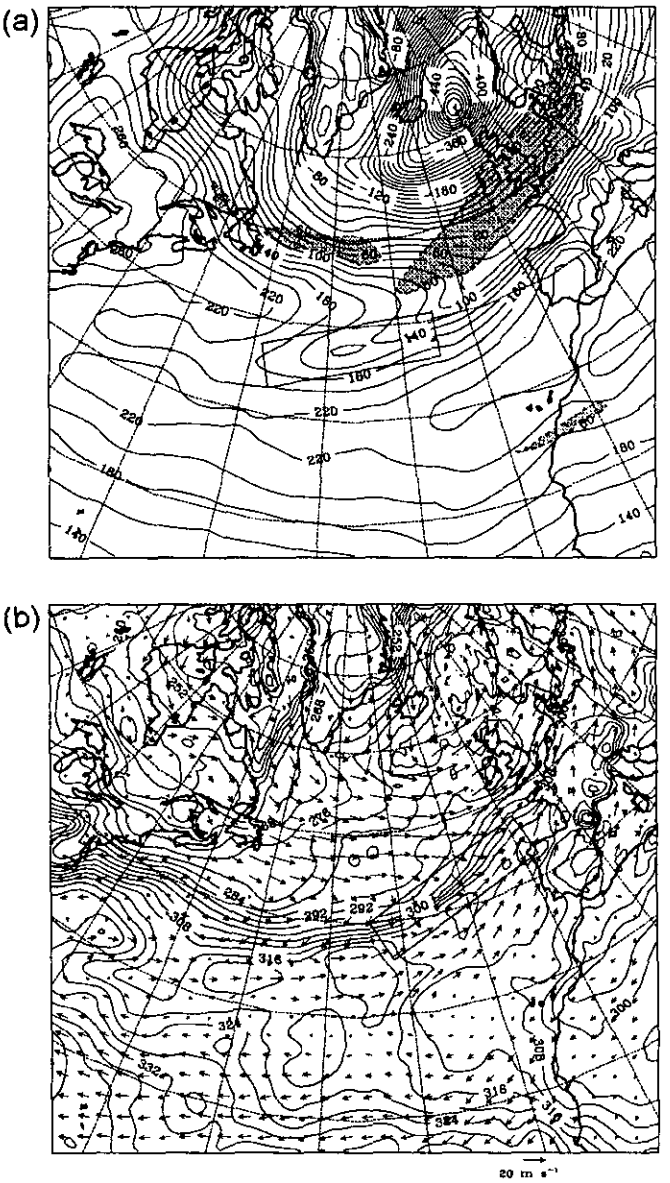

Figure 3. Analysis at 1800 UTC 11 January 1993, as Fig. 1.

of this vapour is instrumental in the formation of the anomalous PV strip along the cold front (shown later).

The main baroclinic wave of the Braer storm is associated with an intense upper-level jet (hereafter called J0) with 300 hPa speeds in excess of 80 m s^{-1}. The surface front evolves under the anticyclonic-shear side of J0 as seen on Figs. 1(a) to 5(a) which show the evolution of the 300 hPa jet core (shaded where greater than 60 m s^{-1}) through the initiation period of the frontal wave. Figure 7 displays a vertical cross-section across the western entrance (i.e. the acceleration area) of J0 and the surface cold front, 6 hours

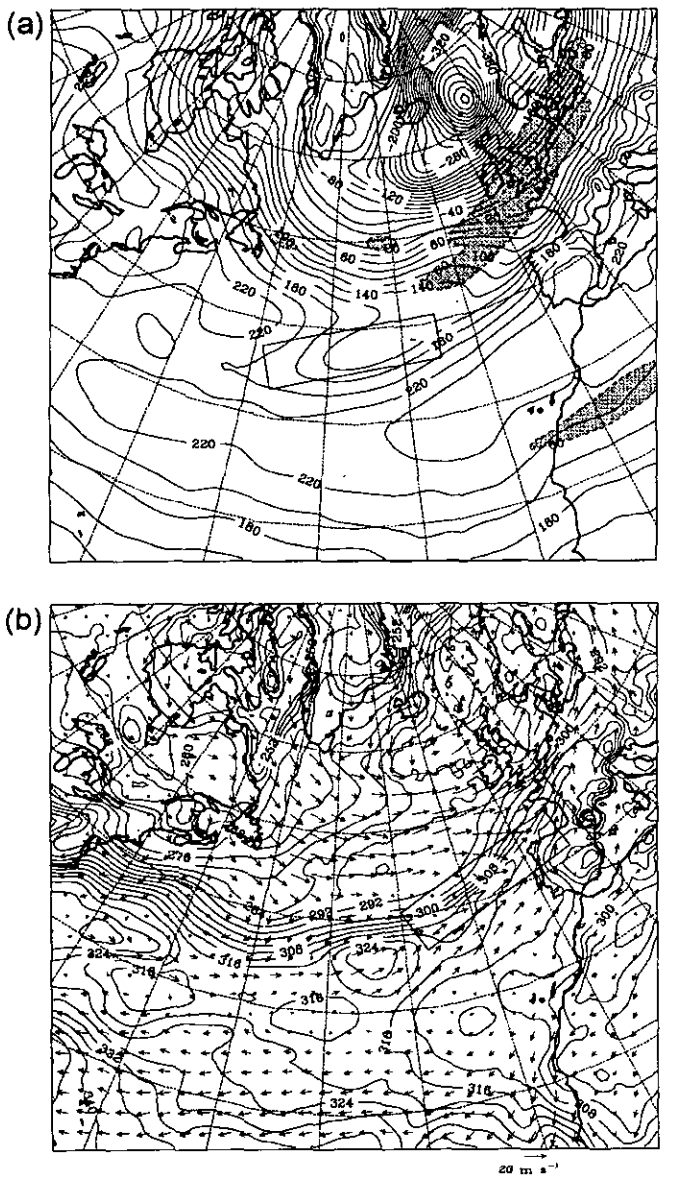

Figure 4. Analysis at 0000 UTC 12 January 1993, as Fig. 1.

before the formation of the frontal wave (see location of the vertical section on Fig. 2(a)). An intense baroclinic zone is associated with the upper-level jet-front system and with the surface front (Fig. 7(a)). A deep tropopause fold is defined by stratospheric-origin values of PV (>1.0 PVU) lying on the cyclonic-shear side of J0 and extending downward to about 600 to 700 hPa (Fig. 7(b)). In the southern part of the vertical cross-section a tower of anomalous PV (0.50–0.75 PVU) extends from the surface to about 400 hPa, coincident with a tower of moist air. These two anomalous zones of PV are embedded in the vertical branches of a very well defined transverse and direct ageostrophic circulation

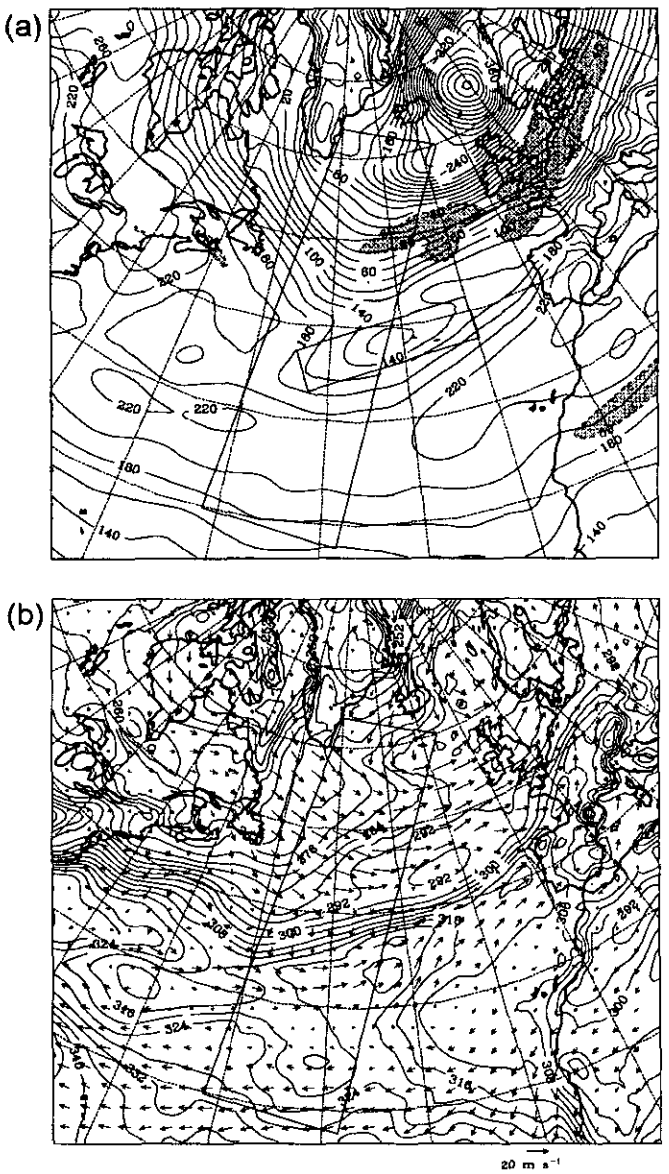

Figure 5. Analysis at 0600 UTC 12 January 1993. As in Fig. 1 except here the path of the DMSP/SSMI orbit is shown for 0830 UTC 12 January 1993.

(TDA) in the entrance area of J0 (Fig. 7(a)). The next section is devoted to a detailed description of the TDA as well as to the investigation of its potential roles in the formation of the frontal wave. To summarize: (i) the cross-frontal ageostrophic convergence at low levels (Fig. 7a) contributes a stabilization of the front through frontogenetic effects; (ii) the upward branch of the TDA (Fig. 7a) lies above the warm side of the cold front and will increase the potential for instability of the front through a diabatic increase of PV; (iii) the tropopause fold (Fig. 7b) may contribute an increase of the potential for instability of the front, through the advection of stratospheric-origin high-PV air into the low-level

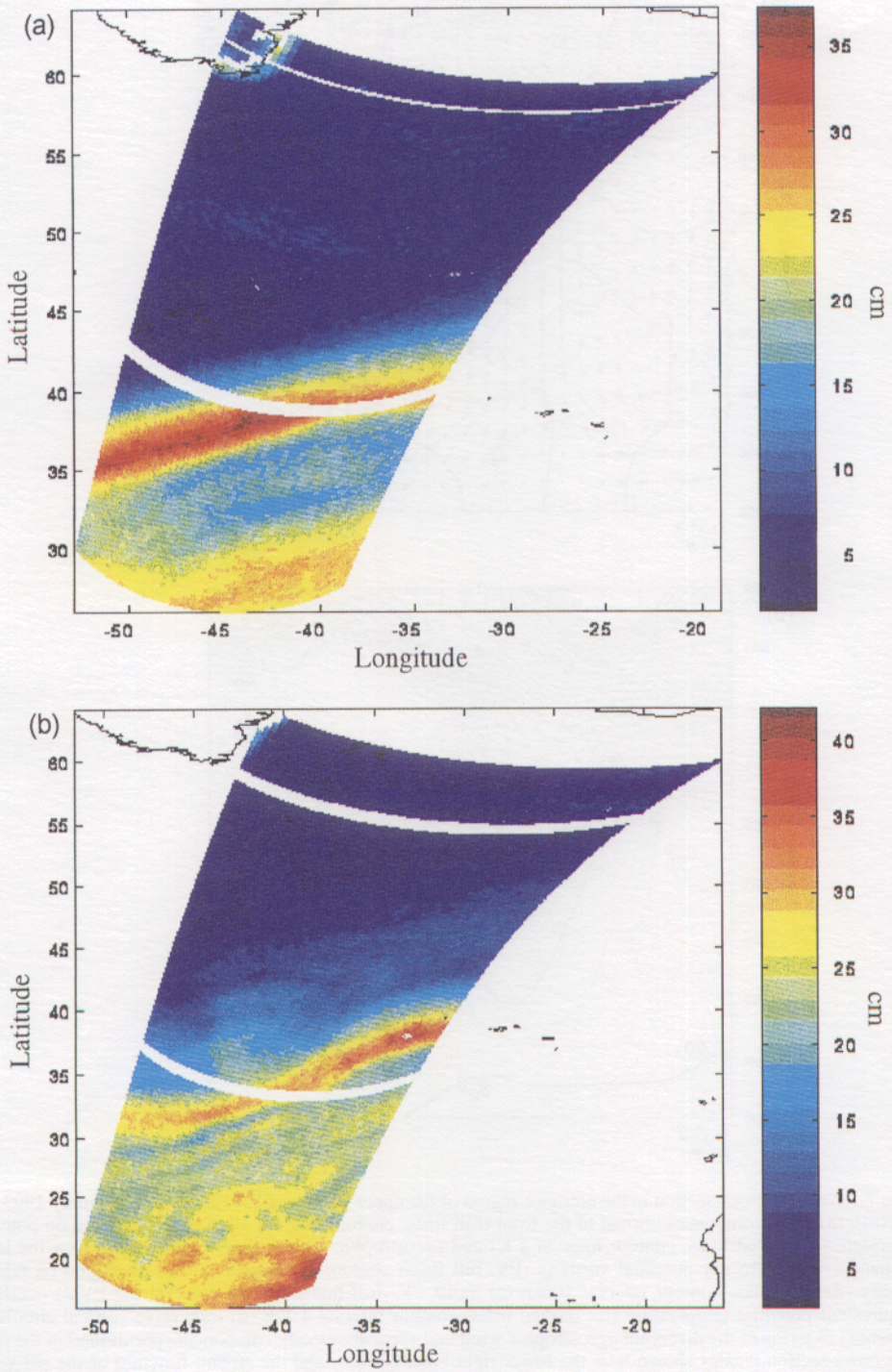

Figure 6. Retrieved DMSP/SSMI (see text) field of Integrated Water Vapour content (IWV) over the sea, in cm (1 cm $\equiv$ 10 kg m^{-2}): (a) 0814 UTC 11 January 1993; (b) 0827 UTC 12 January 1993.

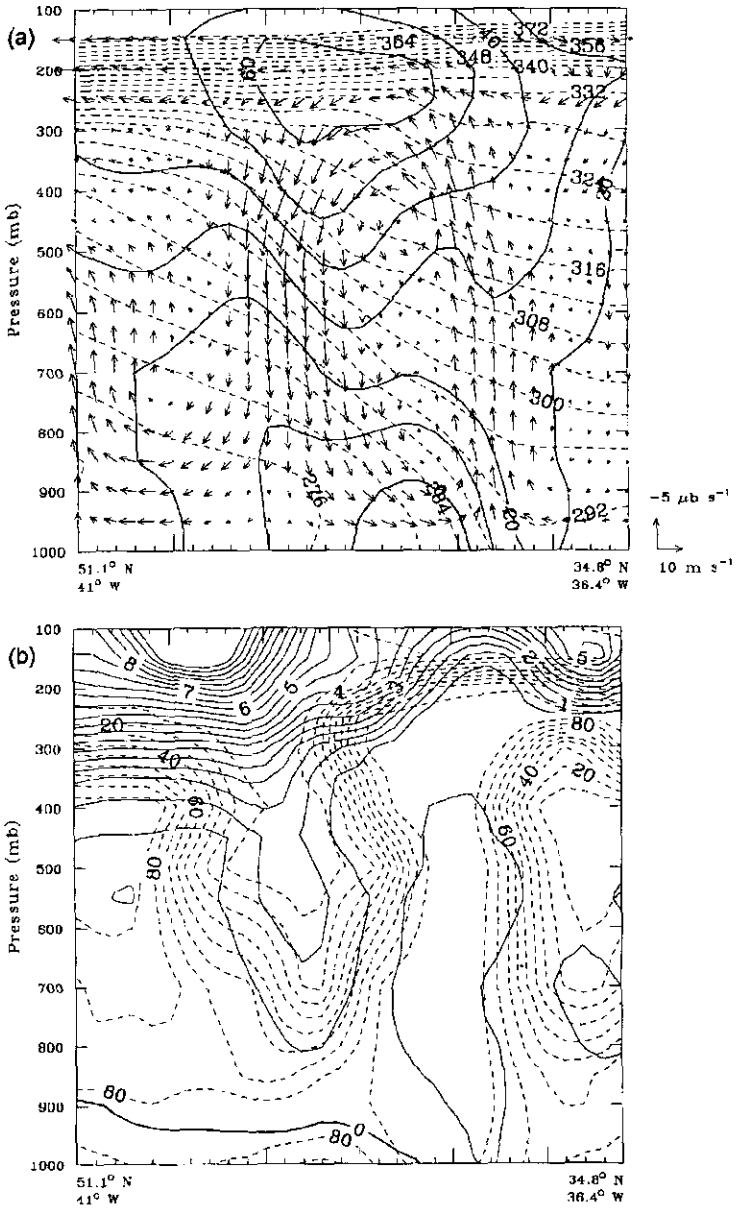

Figure 7. Vertical cross-section in the entrance region of the upper-level jet J0 at 1200 UTC 11 January 1993 (see Fig. 2(a)): (a) wind component normal to the front (full lines; contour interval 10 m s^{-1}) overlayed on potential temperature (θ; dashed lines; contour interval 4 K) and ageostrophic wind vectors (scale shown near the lower right-hand corner); (b) dry potential vorticity (PV; full lines; contour interval 0.5 PVU) overlayed on relative humidity (dashed lines; contour interval 10%); (c) moist PV (full lines; contour interval 0.5 PVU) overlayed on equivalent potential temperature (θ_e; dashed lines; contour interval 4 K); (d) transverse vertical circulation represented in terms of the divergent ageostrophic wind and vertical-velocity components partitioned in the plane of the cross-section (scales shown near the lower right-hand corner), and the stream function of the psi-vector (ψ_s; full lines positive, dashed lines negative; contour interval 4×10^{-2} mb m s^{-1}), overlayed on dry PV where in excess of 0.75 PVU (shaded). Vertical vector wind components (in (a) and (d)) are scaled relative to the horizontal components to be consistent with the respective dimensions of the cross-section. The distance between tick marks on the cross-section abscissa is 75 km measured with respect to the grid. The total distance of 1825 km along the section is measured with respect to the earth. See text for further explanation.

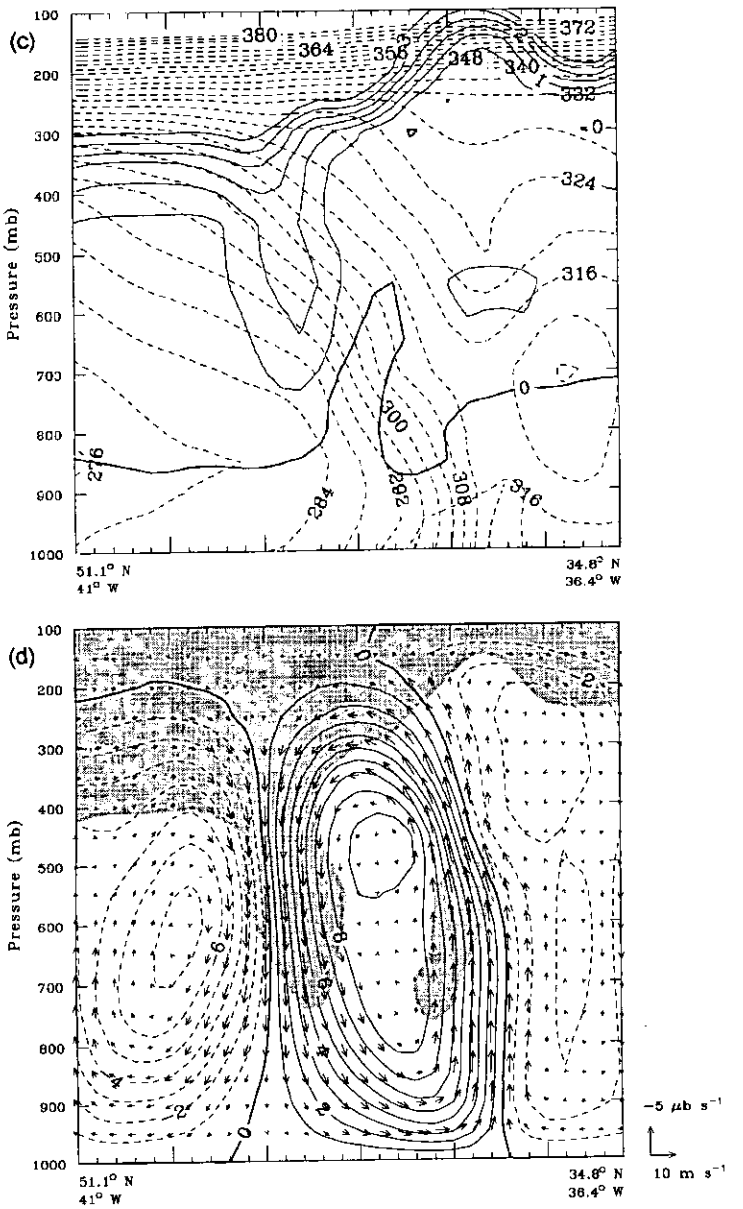

Figure 7. Continued.

baroclinic zone. It is worth noting at this stage of the study, that as the main baroclinic wave fills, both the entrance area of J0 and the associated TDA shift north-eastwards along the surface front. This shift is especially rapid at the time the frontal wave forms (at 1800 UTC 11 January). This can be appreciated by looking at the relative positions of the entrance area of J0 and the western tail of the low-level trough on Figs. 2(a) and 3(a). The timing of the rapid along-front shift hints at the importance of the TDA in the development of the frontal wave.

Briefly turning to the role of the environmental-deformation flow: inspection of low-level wind vectors in the initiation period of the frontal wave (Figs. 1(b) to 5(b)) suggests that: (i) initially a strong stretching-deformation flow is at work on the central-Atlantic part of the cold front (Fig. 1(b)); and (ii) the stretching-deformation rate decreases in the following analyses (Figs. 3(b) to 5(b)). This suggestion is confirmed by the computation of the 1000 hPa total-deformation rate over the Atlantic (not shown): this rate is in excess of 100×10^{-6} s^{-1} at 1200 UTC and is about 50×10^{-6} s^{-1} at 1800 UTC on 11 January. However, as stated by Bishop (1996a,b) and Renfrew *et al.* (1997) the frontal flow may mask the action of the environmental flow on the front. One way to investigate the role of the evolving environmental flow is to partition the flow into frontal and environmental parts using the Bishop attribution technique; this is done in section 3.

(*b*) *Potential for instability of the cold front*

This section examines in more detail the processes associated with the TDA that contribute to the stabilization and to the potential for instability of the cold front. The first of these, the stabilizing effect, is caused by the frontogenetic effects of the cross-frontal convergence at low levels (Fig. 7(a)). In order to better associate this cross-frontal convergence with the TDA, and to show the essentially two-dimensional (2D) character of the latter, we make use of the psi-vector technique (Keyser *et al.* 1989; Loughe *et al.* 1995) to represent the vertical ageostrophic circulation.

Keyser *et al.* (1989) discuss the complications arising in diagnosing transverse ageostrophic circulations in three-dimensional (3D) flows. The method used for diagnosing the TDA in Fig. 7(a) simply uses the cross-front ageostrophic wind and the total vertical velocity. It does not allow any statement on the 2D character of the circulation, as these two components are not linked through a mass-continuity equation. In complicated observational 3D flows a portion of the vertical velocity may not be associated with the divergent flow acting in the cross-front plane, but instead with divergent flow in the along-front plane. This technique partitions the vertical velocity through adoption of a 2D vector stream function, the so-called psi-vector, that represents the divergent ageostrophic circulation in f-plane geometry. The method allows a partition of the vertical circulation into orthogonal vertical planes, forbids the internal cancellation of vertical-velocity components, and ensures that the vertically integrated mass fluxes vanish (for more details see Keyser *et al.* 1989; Loughe *et al.* 1995).

Figure 7(d) displays the circulation vectors of the divergent ageostrophic velocity and the vertical velocity within the cross-section plane, as well as the corresponding stream function component. The circulation agrees well with the one of Fig. 7(a) giving evidence that the TDA is primarily two-dimensional at this time. Such an intense TDA acts in a frontogenetic way on a limited part of the surface front. This part of the front closely corresponds to the zone where parcels move into a region of increased temperature gradient as they enter the upper-level jet. At 1200 UTC 11 January the part of the surface front that undergoes frontogenetic effects from the TDA is roughly at 30–35°W (Figs. 2(a) and 7(d)). Six hours later, the rapid along-front shift of J0 shifts the region of largest low-level cross-frontal convergence to about 20°W, as shown by the 1000 hPa divergent ageostrophic winds (Fig. 8). To visualise the stabilization of the surface front, by the along-front shift of the TDA, one may imagine a zipper going from west to east along the surface front. Any frontal wave under the jet entrance should be flattened by the closing of the zipper. The zipper effect is conceptualized in Fig. 9.

To turn to the role of the TDA in increasing the potential for instability of the cold front, the main feature is the increase in PV of the strip by diabatic processes in the upward branch of the TDA. Figures 7(b)–(c) show a moist and saturated warm sector ahead of

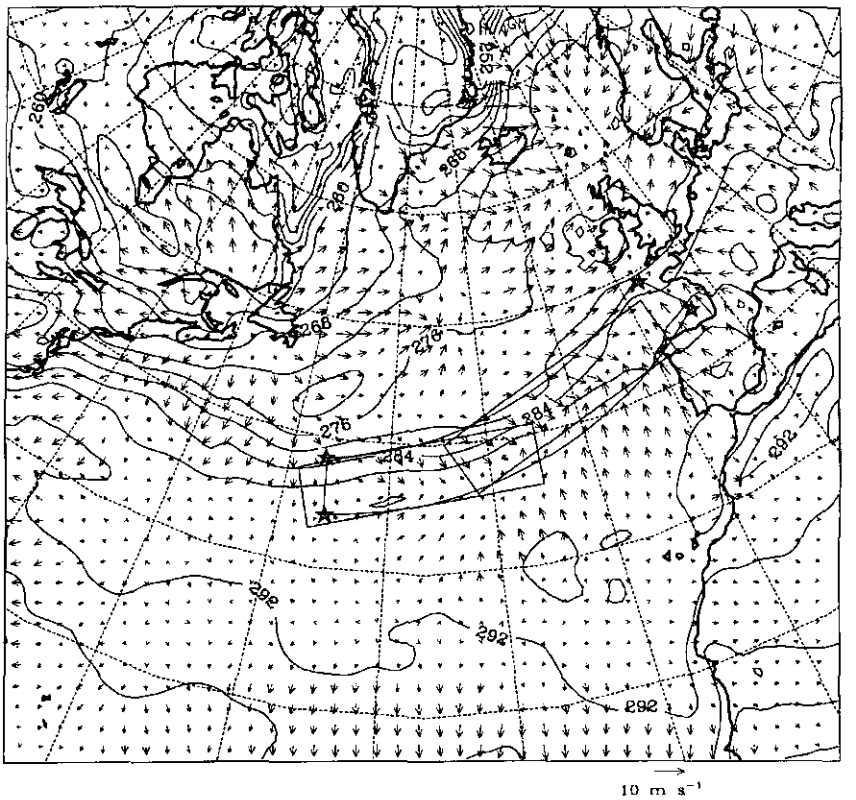

Figure 8. Analysis at 1800 UTC 11 January 1993 showing 1000 hPa divergent ageostrophic wind vectors (scale near the lower right-hand corner), potential temperature (contour interval 4 K), and positions of frontal boxes B1, B2 and B3. The corners of B3 are shown with stars. See text for further explanation.

the cold front. Equivalent-potential-temperature contours indicate convective instability conditions to the north-west of the cross-section. Negative moist PV at the surface front suggests that conditional symmetric instability can exist. These results are consistent with the strong ascent displayed in Fig. 7(a). Vertical gradients of diabatic heating (e.g. latent-heat release) in the upward branch of the TDA must be at work to redistribute the PV, building up a low- and mid-tropospheric tower of positive PV, with a negative cap in the bulge of the tropopause close to the top of the upward branch of the TDA (Fig. 7(b)). At low levels the anomalous PV tower contributes to an increase in the potential for instability of the front.

In order to examine the spatio-temporal dimension of this process, the evolution of the isentropic PV is analysed on the 296 K θ surface that crosses the diabatically produced PV maximum (Fig. 7(b)). Note the 296 K surface also crosses the bottom of the stratospheric-origin PV maximum. The 296 K isentropic PV twelve hours before the frontal wave formation (Fig. 10(a)) exhibits three main features: (i) the polar stratospheric reservoir roughly north of 50°N; (ii) a south-west to north-east tongue of high values (1–2 PVU) near 45°N 40°W, which is the signature of the tropopause fold on the cyclonic-shear side of J0 (see Fig. 1(a)); (iii) a zone of anomalous tropospheric PV (>1.0 PVU) lying over the part of the cold front where the upward branch of the TDA is located at 38°N 48°W. As seen over the following analyses (Figs. 10(b)–(d)) the eastern tip of this tropospheric

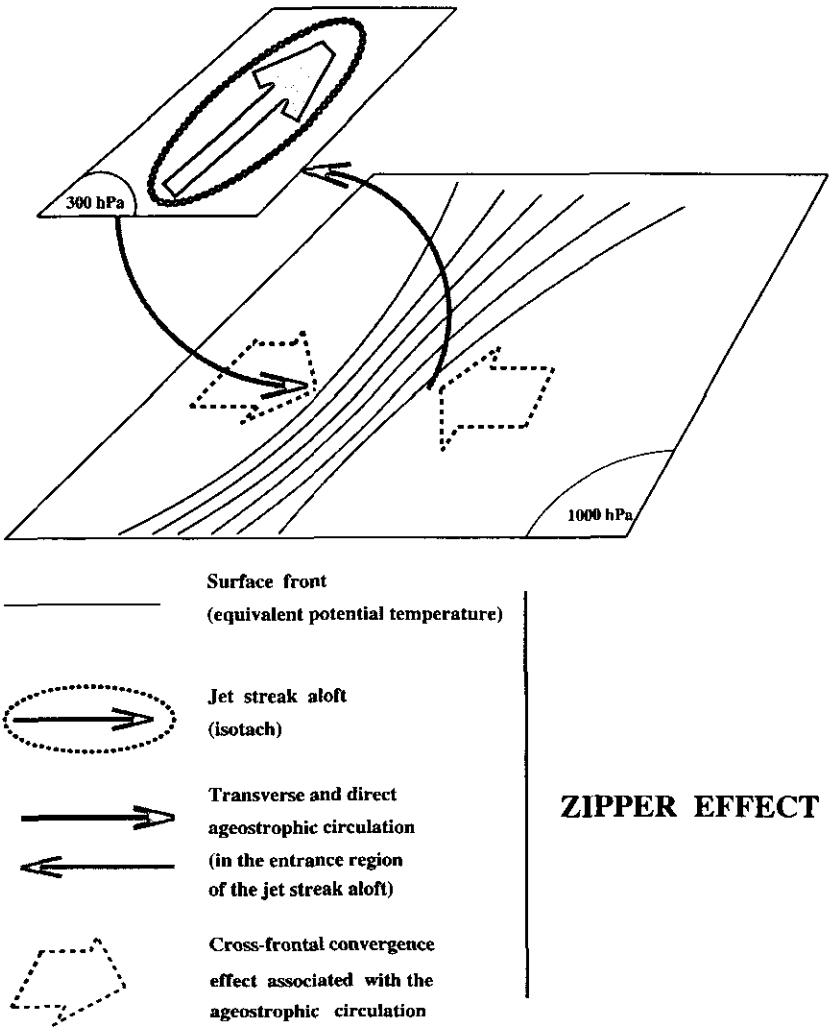

Figure 9. Conceptual view of the 'zipper' effect. Two isobaric planes are shown at 1000 hPa and 300 hPa. The dotted isocontour at 300 hPa represents an isotach of the jet streak with the arrow inside the isotach showing the direction of the jet streak. Isolines on the 1000 hPa surface are of equivalent potential temperature. Curved arrows display the transverse and direct ageostrophic circulation in the vertical cross-front plane in the entrance region of the jet streak. Large dashed arrows symbolize the low-level cross-frontal convergence associated with the ageostrophic circulation. The along-front shift of the ageostrophic circulation makes the frontogenetic low-level cross-frontal convergence resemble a zipper that closes along the front, preventing any frontal wave from developing.

PV zone stretches out in the along-front direction. It is phase-locked with the entrance region of J0. Thus the movement of the upward branch of the TDA contributes to building a quasi-zonal elongated strip of anomalous PV along the cold front.

Looking at the time-evolution of the tropopause-fold signature on the 296 K isentropic PV pattern, it can be seen that the stratospheric-origin tongue is drifting southward as it moves zonally, similar to the conceptualization of Danielsen (1964), or Fig. 15.14 page 435 in Carlson (1991). The junction of the stratospheric-origin tongue and the quasi-zonal elongated strip of diabatic-origin PV along the cold front occurs at 40°N 50°W at 1200 UTC

11 January, i.e. 12 degrees west of the incipient frontal waves and 6 hours before they form. The joining of the two strips of PV with different origins is also accelerated by the cross-frontal-scale contraction undergone by J0 during the saturation phase of the main baroclinic wave (see the width of the jet core in Figs. 1(a) to 5(a)). The TDA at 0600 UTC 11 January is about 800 km wide (Fig. 7(a)) with sloping ascending and subsiding branches. Assuming that the upward and downward branches of the TDA and eastern parts of the PV strips are fixed relative to one another, this width contracts to about 400 km at 1800 UTC 11 January (Fig. 10(c)), whereas in vertical cross-sections (not shown) we note an increasing slope of the ascending and descending branches of the TDA. It therefore seems possible that the tropopause fold has played a role; the superposing of the stratospheric-origin PV and the diabatic-origin PV may contribute to building an unstable structure able to promote a baroclinic growth phase for the frontal wave. Such speculation on the instability of a *'line-tower' of PV developing from a connection between a fold and a lower-level tube* of diabatic-origin PV deserves further investigation. Only the stability of a low-level tube of PV has been studied (Joly and Thorpe 1990). This point is reserved for a subsequent case-study in which a line-tower of PV would clearly emerge from the connection of the two PV strips.

To summarise this section, it has been shown that during the saturation phase of the main baroclinic wave the along-front north-eastward movement of the TDA, at the entrance area of J0, played two conflicting roles on the surface cold front: a stabilizing effect through the low-level cross-frontal convergence; and an increase in the potential for instability, through diabatic redistribution of PV in its upward branch (at the eastern end of the front) and through advection of stratospheric-origin parcels in its downward branch (at the western end of the front). The objective of section 3 is to investigate the role of large-scale deformation and local frontogenesis in triggering the frontal cyclone, using the attribution technique of (Bishop 1996a,b).

3. The role of the environmental flow

(a) *The domain-independent attribution method*

A domain-independent vorticity and divergence attribution technique has been developed by Bishop (1996a,b) and applied in several frontal cyclone cases by Renfrew *et al.* (1997). Readers are referred to these studies for the technical details of the technique. A short summary is given here.

The partitioning of a horizontal wind field into irrotational and nondivergent parts, on a finite domain, is achieved by solving the Poisson equations, for the stream function from vorticity and the velocity potential from divergence, using free-space Green's functions. These remove the boundary conditions to infinity, and so give a certain domain independence to the stream function and velocity-potential solutions. Each grid point of the domain is associated with a disc of uniform vorticity and a disc of uniform divergence, calculated from circulation and flux estimates of the neighbouring grid boxes. Each element of vorticity and divergence is therefore associated with a unique wind field, obtained via the Poisson equation solutions. The flow obtained by summing the winds induced by all the elements of vorticity in the finite domain defines the total rotational flow, u_ψ. Similarly, summing the winds induced by all the elements of divergence in the finite domain gives the divergent flow, u_χ. The 'remainder' harmonic part of the wind, u_ϑ, is both solenoidal and irrotational in the finite domain, and is due to vorticity and divergence outside of the domain. This three-component partition of the observed wind ($u_{\text{obs}} = u_\psi + u_\chi + u_\vartheta$) is unique and independent of the domain boundaries.

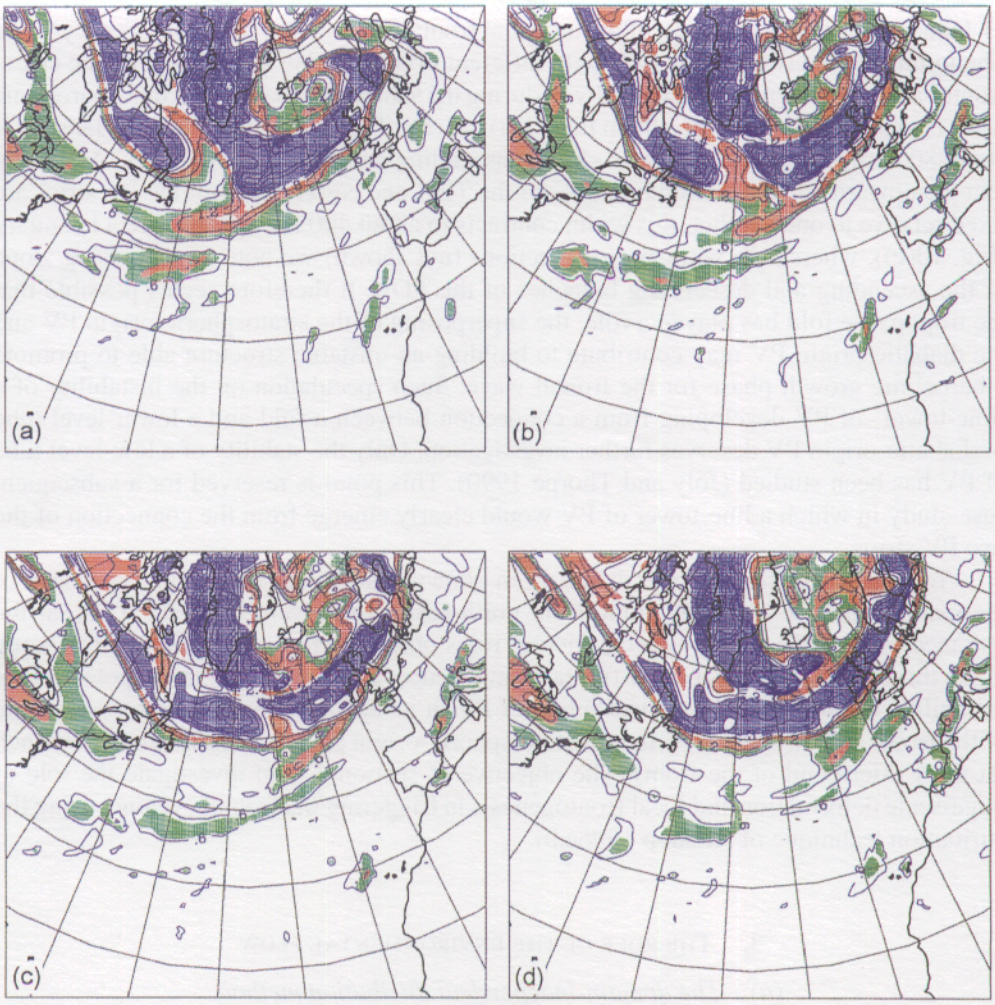

Figure 10. Isentropic potential vorticity (PV) for potential temperature $\theta = 296$ K. The lowest isocontour plotted is 0.6 PVU, green values indicate 0.7 PVU < PV < 1.0 PVU, red values indicate 1.0 PVU < PV < 2.0 PVU, blue values indicate PV > 3.0 PVU: (a) 0600 UTC 11 January 1993; (b) 1200 UTC 11 January 1993; (c) 1800 UTC 11 January 1993; (d) 0000 UTC 12 January 1993.

Bishop (1996b) proposes a piecewise-like methodology to partition the observed flow into a frontal part and an environmental part, by defining a 'frontal box' around a limited part of the surface front. The frontal flow (u_i) is defined as the wind induced by the vorticity elements ($u_{i\psi}$) and divergence elements ($u_{i\chi}$) inside the ith frontal box. The environmental flow is the external flow (u_e) induced by vorticity elements ($u_{e\psi}$) and divergence elements ($u_{e\chi}$) external to the frontal box, and vorticity and divergence elements outside the finite domain (u_ϑ); so that ($u_{obs} = u_e + u_i = (u_{e\psi} + u_{e\chi} + u_\vartheta) + u_{i\psi} + u_{i\chi})$). All computations of wind derivatives are done in a frontal co-ordinate system with (x_f, y_f) the across-front and the along-front directions respectively. The long sides of the box are in the along-front direction, and for a cold front the across-front direction points towards the warm air. The along-front stretching due to the environmental flow is then defined by $\gamma_e = \partial v_e / \partial y_f$ where v_e is the along-front component of the environmental wind. Values of γ_e are then averaged in the central part of the frontal box, excluding all data within 7×75 km of the ends in order to avoid contributions of frontal vorticity and divergence lying close to the border

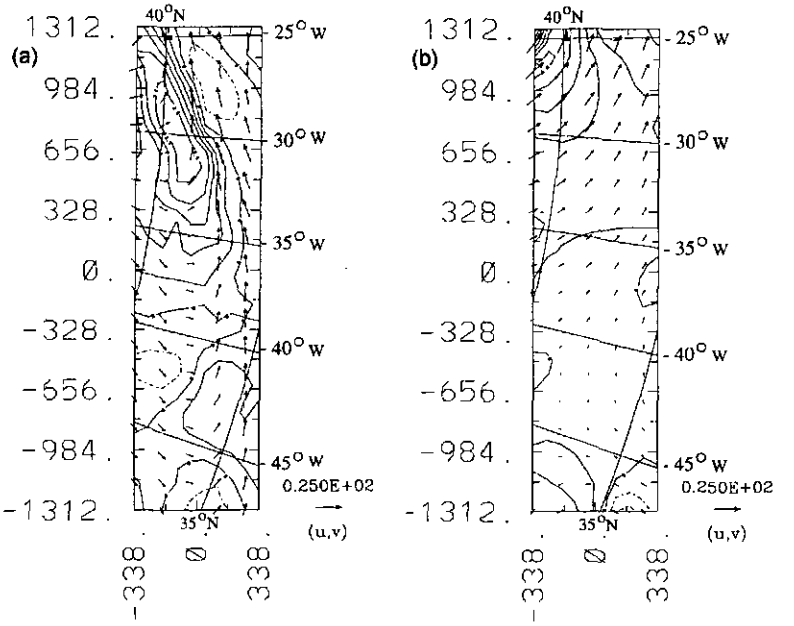

Figure 11. Frontal box B1 at 1800 UTC 11 January 1993: (a) observed wind vectors (scale given near the lower right-hand corner) and along-front stretching from the observed wind $\gamma_{obs} = \partial v_{obs}/\partial y_f$ (contour interval 0.5×10^{-5} s^{-1}); the average value in the central part of the box is 0.591×10^{-5} s^{-1}. (b) environmental wind vectors (scale near the lower right-hand corner) and along-front stretching from the environmental wind $\gamma_e = \partial v_e/\partial y_f$ (contour interval 0.5×10^{-5} s^{-1}); the average value in the central part of the box is 0.424×10^{-5} s^{-1}. In both (a) and (b) axes are labelled in km. See text for further explanation.

of the frontal box. This average along-front stretching will be compared to its counterpart, the large-scale deformation used in idealized models (Drischel *et al.* 1991; Bishop and Thorpe 1994b).

As an example, Figs. 11(a) and 11(b) show the distribution of the observed and environmental along-front stretching within the frontal box B1 (to be defined later) i.e. $\partial v_{obs}/\partial y_f$ and $\partial v_e/\partial y_f$ respectively. The benefits of the attribution technique are seen in the smooth aspect of the distribution of the environmental along-front stretching. It avoids contributions from local structures as seen in the distribution of the observed along-front stretching. Sensitivity aspects for the frontal box size and position relative to the front, are shown to be about 10% for the average along-front environmental stretching (Renfrew 1995; Renfrew *et al.* 1997). The strategy employed in defining the frontal boxes in the present case-study is discussed in section 3(b).

Bishop (1996b) uses the attribution technique to distinguish frontogenesis due to the environmental flow from that due to the frontal shear. Following Keyser *et al.* (1988) he defines F_0 as the Lagrangian rate of change of the horizontal potential-temperature gradient due to horizontal advection:

$$F_0 = -((\partial u_{0f}/\partial x_f\ \partial\theta/\partial x_f) + (\partial v_{0f}/\partial x_f\ \partial\theta/\partial y_f),$$
$$(\partial u_{0f}/\partial y_f\ \partial\theta/\partial x_f) + (\partial v_{0f}/\partial y_f\ \partial\theta/\partial y_f))$$

where u_{0f} and v_{0f} represent the across- and along-front components of the wind, respectively. This is the vector frontogenesis function. Substituting the above wind partition, the observed frontogenesis vector can be split in the following way: $F_0 = F_e + F_{i\psi} + F_{i\chi}$,

where F_e, $F_{i\psi}$, $F_{i\chi}$ represent frontogenesis due to the environmental flow u_e, the local horizontal shear $u_{i\psi}$ and the local ageostrophic circulation $u_{i\chi}$, respectively. In this study, we use the attribution technique to survey the time-evolution of the frontogenetic cross-frontal convergence on different parts of the surface cold front, by computing the frontogenesis due to the local ageostrophic circulation $F_{i\chi}$. As noted earlier the front has a well-defined gradient of temperature (Fig. 8), so examining the three frontogenetic components allows the relative importance of ageostrophic convergence to be assessed over time.

(*b*) *Lagrangian strategy with frontal boxes*

Theoretical results (Dritschel *et al.* 1991; Bishop and Thorpe 1994) and case-study results (Renfrew *et al.* 1997) indicate that the capacity for frontal waves to develop along fronts may depend significantly on the time-dependent along-front stretching. To investigate this, a first frontal box, B1, is defined to be phase-locked with the frontal wave and aligned with the vorticity contours (not shown) approximately parallel to the equivalent-potential-temperature contours in this case. From 1800 UTC 11 January (the key date of the formation of the frontal wave) to 0600 UTC 12 January, the centre of B1 is phase-locked with the minimum of geopotential along the tail of the surface trough. Before the key date (0600 UTC and 1200 UTC 11 January), since no 1000 hPa geopotential minimum is observed along the front, the position of B1 is determined relative to a box B2 (defined below). The along-front long sides of B1 are 35 × 75 km, the width is 9 × 75 km and the box encompasses the equivalent-potential-temperature gradient. Successive positions of B1 are shown on Figs. 1(a) to 5(a). The geometric parameters of the frontal boxes are given in Table 1.

The objectives in choosing another two boxes, B2 and B3, are to analyse the spatio-temporal variations of the stabilizing and destabilizing processes along the entire surface front. These are twofold: (i) to confirm the stabilizing role of the low-level cross-frontal convergence by quantifying its contribution to the total frontogenesis; and (ii) to evaluate the geographical variation along the surface front of the environmental along-front stretching. The frontal box B2 is defined to be phase-locked with the TDA; the criterion to position it, is to follow the maximum crest line of the low-level ageostrophic convergence (Fig. 8). Like B1, box B2 is aligned with vorticity contours and has identical dimensions to B1. Successive positions of B2 are represented on Figs. 1(b) to 5(b). Note B1 and B2 have identical geographical locations at 0600 UTC 11 January. Box B1 at 1200 UTC 11 January is in an intermediate position from those defined 6 hours either side of it. The third box, B3, is defined to encompass the two other boxes and covers most of the length of the surface front. All three boxes are shown at 1800 UTC 11 January on Fig. 8. B1 and B2 are rectangular; B3 is defined as a segment of an annulus, in order to encompass the curved front.

All of the results quoted in this paper were obtained using 1000 hPa winds. Bishop (1996b) and Renfrew *et al.* (1997) used 900 hPa winds in order to avoid the boundary-layer problems that could occur, especially over land. In our case-study, sensitivity tests using pressure levels up to 700 hPa, which would be above the marine boundary layer over

TABLE 1. CHARACTERISTICS OF THE FRONTAL BOXES.

	Width (km)	Length (km)	Type	Length of the averaging zones (km)
B1 & B2	675	2625	rectangle	1575
B3	675	4875	annulus sector	3825

most oceanic regions, show little numerical differences in average values of along-front stretching. The quite similar time-evolutions emphasize relatively homogeneous behaviour of the environmental stretching in the 1000–700 hPa layer. Hence we present our results on the 1000 hPa level, as this is consistent with our criterion for defining the frontal wave from the 1000 hPa geopotential height. Note that computations of wind derivatives for B2 and B3 are not performed for the last time period of the case-study (0600 UTC 12 January) as the surface front moves over land. As in Renfrew (1995) tests performed by varying the width of the frontal boxes did not show any large sensitivities.

(c) *Large-scale deformation and local frontogenesis evolutions*

Table 2 shows the time-evolution of the average along-front stretching of the observed wind, γ_{obs}, and of the along-front stretching of the environmental wind, γ_e, in the frontal box B1. It is clear that γ_{obs} undergoes a rather erratic variation which displays no coherent trend; solving this problem was the main motivation for Bishop (1996a,b) to create the domain-independent attribution technique. Renfrew *et al.* (1997) explain this effect by noting the inconsistent sampling, over time, of the small-scale structure that appears in the pattern of γ_{obs} (e.g. Fig. 11(a)), and noting also that the observed stretching will be sensitive to the chosen along-front direction of the frontal box. These two factors mean the observed along-front stretching values are largely meaningless. In contrast, the much smoother and uniform pattern of γ_e (Fig. 11(b)) allows one to extract a clear background signal. The environmental stretching γ_e, undergoes a monotonic decrease over the 24-hours. Furthermore, γ_e is below the critical threshold γ_c, defined by Bishop and Thorpe (1994b), except for the very first time period shown (0600 UTC 11 January). The decrease in the observed stretching fits in well with the scenario outlined earlier (Bishop and Thorpe 1994b, Renfrew *et al.* 1997) of strong stretching initially, and a falling-off with time.

Figure 12 shows the time-evolution of γ_e for all three boxes. From the evolution of γ_e in the largest box, B3, it can be concluded that the environmental along-front stretching is falling along the whole front. The delayed fall of γ_e for B2 may be explained by its more easterly position—closer to the primary cyclone of the Braer storm. Which part of the primary cyclone could be associated with this delay may be inferred by thinking of a simple PV based model of an upper-level jet streak, i.e. a dipole of PV at upper levels, where each advects the other along. The wind field attributable to these PV anomalies would affect the low-level along-front stretching. In particular, as J0 moved into the north-eastern sector of B2, the PV anomalies associated with the jet streak would contribute positively to the 1000 hPa along-front stretching in B2, explaining the delayed fall of γ_e in this region. This is the kind of assumption that could be checked in further work with a PV inversion method. In short, it seems the whole surface front undergoes a fall in

TABLE 2. TIME EVOLUTION OF THE AVERAGED ALONG-FRONT STRETCHING OF THE OBSERVED AND ENVIRONMENTAL WINDS THROUGH THE CASE-STUDY PERIOD IN BOX B1.

	Average along-front stretching	
	γ_{obs}	γ_e
06 UTC 11 JAN	0.14 E−05	0.61 E−05
12 UTC 11 JAN	0.54 E−05	0.44 E−05
18 UTC 11 JAN	0.59 E−05	0.42 E−05
00 UTC 12 JAN	0.26 E−05	0.25 E−05
06 UTC 12 JAN	0.16 E−05	0.17 E−05

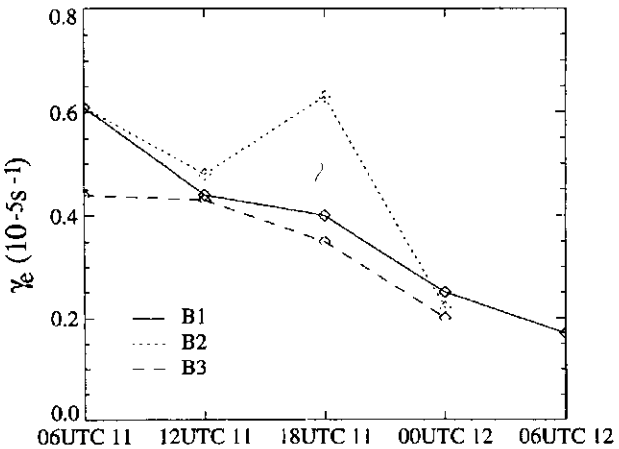

Figure 12. Along-front environmental stretching rates $\gamma_e(10^{-5}\ s^{-1})$ for frontal boxes B1, B2 and B3 (see text) throughout the case-study period. The plotted values are averages over the central part of the frontal boxes.

TABLE 3. TIME-EVOLUTION OF COMPONENTS OF FRONTOGENESIS VECTOR IN BOX 1 EXPRESSED AS PERCENTAGES OF THE TOTAL

		Frontogenetic components		
	F_0	F_e/F_0	$F_{i\psi}/F_0$	$F_{i\chi}/F_0$
06 UTC 11 JAN	(4.0, 0.6) E−10	33	3	65
12 UTC 11 JAN	(3.0, 0.9) E−10	23	14	63
18 UTC 11 JAN	(1.7, 0.1) E−10	35	24	41
00 UTC 12 JAN	(1.2, 0.3) E−10	25	17	58
06 UTC 12 JAN	(1.5, 0.3) E−10	13	20	67

environmental along-front stretching below the critical threshold, and so would be able to release its potential for instability to form a wave. We therefore have to find a reason for the formation of the frontal wave *in the box B1*.

Table 3 gives the time-evolution of the frontogenesis vector components from the observed wind field. The across-front component clearly dominates the along-front one and decreases over time, hence the following discussion deals only with the across-front frontogenetic components. To be precise, Table 3 displays the total across-front frontogenesis, F_0, and components due to: the environmental flow F_e; the local horizontal shear $F_{i\psi}$; and local convergence $F_{i\chi}$, each expressed as a percentage of F_0. All ratios are for B1. In this case $F_{i\chi}/F_0$ is the dominant contributor; that is to say the ageostrophic convergence provides the largest contribution to the total frontogenesis. The contribution is at a minimum (41%) at 1800 UTC 11 January—the key time for the frontal wave formation. This corresponds to the time the TDA moves out of B1 (Fig. 3(a) and Fig. 8). Six hours later the increase in this contribution could be attributed to local frontogenetic processes in the development phase of the frontal wave. Keeping B2 phase-locked with the low-level branch of the TDA maintains a constant and strongly dominant contribution to frontogenesis from the low-level ageostrophic convergence (Fig. 13); this is the zipper effect mentioned earlier. On the basis of the time-evolution of the environmental along-front stretching and the contribution to frontogenesis in B1 and B2, it is clear that the frontal wave grows *when* the large-scale deformation field decays and *where* the stabilizing frontogenesis due to the TDA decays.

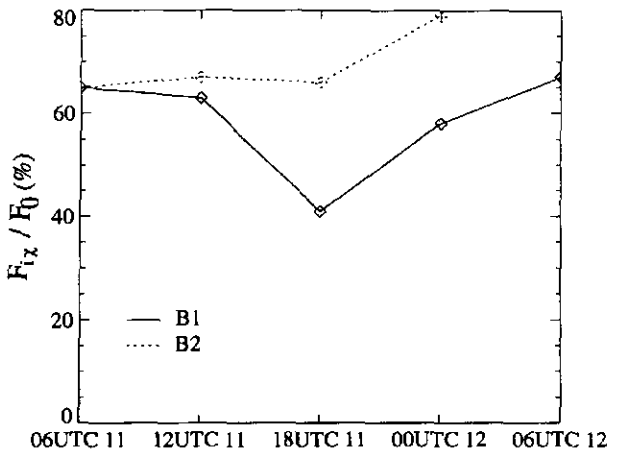

Figure 13. Contribution (%) of the local ageostrophic circulation flow to the observed frontogenesis ($F_{i\chi}/F_{obs}$) in frontal boxes B1 and B2 throughout the case-study period. See text for details.

(*d*) *Discussion*

Estimates of frontogenesis due to ageostrophic convergence are dependent on the spatial resolution of the observation and assimilation system used to produce the ECMWF analyses. The above results are presented using the operational ECMWF analyses, i.e. at T213 truncation. To investigate the horizontal-resolution dependency, the domain-independant attribution method has also been applied to ECMWF analyses with truncations of T106 and T63 for box B1 on 11 January 1993 at 1200 UTC and 1800 UTC. Results show that the frontogenesis due to ageostrophic convergence is more sensitive to the horizontal resolution than the frontogenesis due to horizontal shear. The ageostrophic-convergence frontogenetic contribution is found to decrease when degrading the horizontal resolution. Errors associated with estimates of mesoscale frontogenetic forcings (ageostrophic convergence and horizontal shear) are small, 4%, with the T106 truncation, but increase up to 10% using the T63 truncation. Very little sensitivity is found in the environmental contribution when using the T106 fields; with the T63 fields the environmental average along-front stretching tends towards the observed average along-front stretching. This means that there is little justification in applying the domain-independent attribution method to such a problem with a T63 horizontal resolution. It thus seems that, from the results of these sensitivity tests, the errors associated with the estimates of frontogenesis due to ageostrophic convergence are reasonable.

In this case-study the reduction in frontogenesis due to ageostrophic convergence is significant at a key time for frontal wave development, while the reduction in environmental stretching is continuous over the period. This raises the question—which of these two indicators might correlate better with frontal wave development? To answer this, and confirm our choice of key date for the frontal wave triggering, a second measure of frontal wave growth, the 'vorticity-waviness' defined by Renfrew *et al.* (1997), is computed. The vorticity-waviness is defined as the peak vorticity minus the maximum along-front average vorticity of the front in the box. Figure 14 displays the time-evolution of the vorticity-waviness as well as the maximum along-front average vorticity in B1. The vorticity-waviness increases from 1.0×10^{-4} s^{-1} to 1.3×10^{-4} s^{-1} throughout the period studied, with a peak value of 1.4×10^{-4} s^{-1} at 1800 UTC 11 January. This is the date we defined for the formation of the frontal wave and reinforces our choice. Note the average along-front

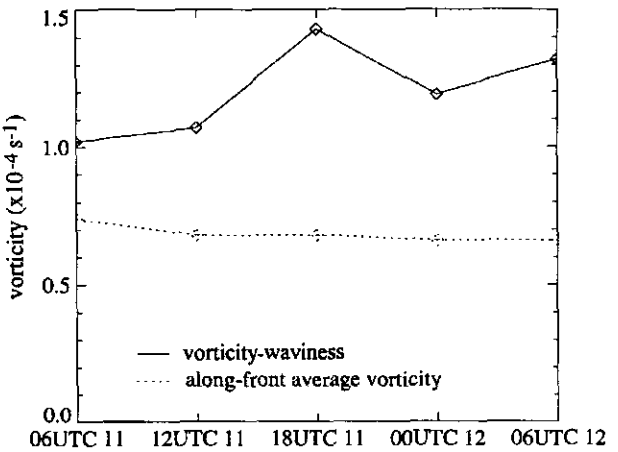

Figure 14. Vorticity-waviness and maximum along-front averaged vorticity (10^{-4} s^{-1}) from 0600 UTC 11 January to 0600 UTC 12 January in box B1 and at 1000 hPa. See text for details.

vorticity is approximately constant throughout the period, indicating maintenance of the vorticity front. The growth estimation of the frontal wave (measured as the rate of change of vorticity-waviness) equals 1.8×10^{-9} s^{-2} at 1800 UTC 11 January, which is a coherent value for frontal waves growing in weak environmental stretching deformation (Renfrew *et al.* 1997, their Fig. 15). Thus, it appears our earlier contention that the frontal wave grows *when* the large-scale deformation field decays, and *where* the stabilizing frontogenesis due to the TDA decays, is corroborated by an examination of the vorticity distribution.

It should be noted that Bishop and Thorpe (1994a,b) offer theoretical arguments to link these two indicators. They point out that in a balanced semi-geostrophic type of frontogenesis, the integral over the cross-frontal plane of the frontogenesis due to environmental along-front stretching is directly proportional to the ageostrophic cross-frontal circulation, and hence, indirectly, to the strength of the frontogenesis due to ageostrophic convergence. Thus, one would be justified in interpreting a decrease in frontogenesis due to ageostrophic convergence as an indication of a decrease in the vertically averaged along-front stretching rate, in the straightforward case. This can, however, be complicated by changes in the temperature distribution and the influence of frontogenetic horizontal shear. In addition, the flow at fronts will be out of balance at times, in which case these arguments break down. It does seem clear though that both environmental deformation and ageostrophic convergence should be examined to determine the likelihood that a front will develop waves.

Another interesting question that has arisen from this study is the precise nature of the influence of the upper-level jet on the frontal wave, and if that affects the environmental deformation. A more detailed investigation would also shed some light on the less clear-cut role that environmental deformation flows play in the development of baroclinic disturbances (Bishop 1993). These questions must be reserved for a future study, perhaps using the wealth of FASTEX data now available.

4. Conclusion

The initiation phase of a frontal wave over the Atlantic (11–12 January 1993) has been investigated. The frontal wave chosen develops in the wake of a major primary cyclogenesis event that broke the record for low pressure over the Atlantic. Evidence is

shown of two conflicting roles for the transverse and direct ageostrophic circulation (TDA) lying in the entrance region of an intense upper-level jet associated with the primary cyclogenesis. The circulation stabilizes the surface front, through frontogenetic cross-frontal low-level convergence (the 'zipper' effect); but also (potentially) destabilizes the front, as the upward branch of the circulation increases the potential for instability through diabatic PV redistribution. In other words the TDA locally stabilizes the surface front but also builds up an elongated strip of anomalous PV.

In addition evidence is shown of the connection between a tropopause fold, embedded within the subsiding branch of the TDA, and the low-level elongated strip of diabatic-origin PV. The importance of this connection in building an unstable PV structure, able to promote a baroclinic growth phase for the frontal wave, deserves further investigation.

The following scenario is tested: once the potential for instability of the front has been increased and stabilizing effects become small, the frontal cyclone is free to grow. Using a domain-independent attribution method (Bishop 1996a,b) it has been shown that the frontal wave forms on a part of the cold front: *where* the along-front stretching due to the environment flow decays below the critical threshold value ($\gamma_c = 0.6 \times 10^{-5}$ s^{-1}) prescribed by theoretical studies (Bishop and Thorpe 1994a,b); and *when* the across-front frontogenesis component due to the ageostrophic circulation decays. This is a coherent result in the framework of semi-geostrophic theory, where cross-frontal convergence and stretching deformation are linked through the Sawyer–Eliassen equation. Our results fit well with the conclusions of Renfrew *et al.* (1997) and put on a firmer observational basis the theoretical ideas of Bishop and Thorpe (1994a,b). It seems that the potential for instability (i.e. the PV strip), the evolving environmental flow and the induced ageostrophic convergence all have a crucial role in differentiating growth from suppression of frontal waves. Detailed case-studies of frontal waves like the one in this paper were of vital importance in preparing final observational strategies in the build up to the 1997 FASTEX experiment.

Acknowledgements

This work was supported by the Programme Atmosphère Météorologique et Océan Superficiel at the Institut National des Sciences de l'Univers. We would like to thank Craig Bishop for providing us with his attribution software. Craig Bishop and another anonymous reviewer are acknowledged for their thorough reviews. Helpful comments from Alain Joly and Alan Thorpe were greatly appreciated.

References

Ayrault, F., Lalaurette, F., Joly, A. and Loo, C. 1995 North Atlantic ultra high frequency variability: An introduction survey. *Tellus*, **47A**, 671–696

Bishop, C. H. 1993 On the behaviour of baroclinic waves undergoing horizontal deformation. II: Error-bound amplification and Rossby wave diagnostics. *Q. J. R. Meteorol. Soc.*, **119**, 241–267

1996a Domain independent attribution. I: Reconstructing the wind from estimates of vorticity and divergence using free space Greens functions. *J. Atmos. Sci.*, **53**, 241–252

1996b Domain independent attribution. II: Its value in the verification of dynamical theories of frontal waves and frontogenesis. *J. Atmos. Sci.*, **53**, 253–262

Bishop, C. H. and Thorpe, A. J. 1994a Frontal wave stability during moist deformation frontogenesis. Part I: Linear wave dynamics. *J. Atmos. Sci.*, **51**, 852–873

1994b Frontal wave stability during moist deformation frontogenesis. Part II: The suppression of nonlinear wave development. *J. Atmos. Sci.*, **51**, 874–888

Browning, K. A. and Roberts, N. M.	1994	Structure of a frontal cyclone. *Q. J. R. Meteorol. Soc.*, **120,** 1535–1557
Carlson, T. N.	1991	*Mid-latitude weather systems.* Harper Collins Academic, London
Charney, J. G. and Stern, M. E.	1962	On the stability of internal baroclinic jets in a rotating atmosphere. *J. Atmos. Sci.*, **19,** 159–162
Danielsen, E. F.	1964	'Report on Project Springfield'. DASA 1517, HQ, Defense Atomic Support Agency. Washington, D.C.
Dritschel, D. G., Haynes, P. H., Juckes, M. N. and Shepherd, T. G.	1991	The stability of a two-dimensional vorticity filament under uniform strain. *J. Fluid Mech.*, **230,** 647–665
Farrell, B. F.	1984	Modal and non-modal baroclinic waves. *J. Atmos. Sci.*, **41,** 668–673
	1989	Optimal exitation of baroclinic waves. *J. Atmos. Sci.*, **46,** 9, 1193–1206
Fehlmann, R. and Davies, H. C.	1997	Misforecasts of synoptic systems: diagnosis via PV-retrodiction. *Mon. Weather Rev.*, **125,** 2247–2264
Hewson, T. D.	1993	'The FRONTS 92 experiment: a quicklook atlas'. Internal report No. 15. Available from JCMM, University of Reading, UK
Hoskins, B. J.	1975	The geostrophic momentum approximation and the semi-geostrophic equations. *J. Atmos. Sci.*, **32,** 233–242
Hoskins, B. J. and Berrisford, P.	1988	The storm of 15–16th October 1987: A potential vorticity perspective. *Weather*, **43,** 122–129
Hoskins, B. J. and Bretherton, F. P.	1972	Atmospheric frontogenesis models: Mathematical formulation and solution. *J. Atmos. Sci.*, **29,** 11–37
Jarraud, M., Goas, J. and Deyts, C.	1989	Prediction of an exceptional storm over France and southern England (15–16 October 1987), *Weather and Forecasting*, **4,** 517–536
Joly, A.	1995	The stability of steady fronts and the adjoint method: Non-modal frontal waves. *J. Atmos. Sci.*, **52,** 3082–3108
Joly, A. and Thorpe, A. J.	1990	Frontal instabilities generated by tropospheric potential vorticity anomalies. *Q. J. R. Meteorol. Soc.*, **116,** 525–560
	1991	The stability of time-dependent flows: an application to fronts in developing baroclinic waves. *J. Atmos. Sci.*, **48,** 163–182
Joly, A., Thorpe, A. J., Lemaitre, Y., Browning, K. and Lalaurette, F.	1994	'FASTEX (Fronts and Atlantic Storm Tracks EXperiment).' Scientific papers. Available from the FASTEX Project Office, Toulouse, France
Joly, A., Jorgensen, D., Shapiro, M. A., Thorpe, A., Bessemoulin, P., Browning, K. A., Cammas, J.-P., Chalon, J.-P., Clough, S. A., Emanuel, K. A., Eymard, L., Gall, R., Hildebrand, P. H., Langland, R. H., Lemaitre, Y., Lynch, P., Moore, J. A., Persson, P. Ola G., Snyder, C. and Wakimoto, R. M.	1997	Definition of the Fronts and Atlantic Storm-Track Experiment (FASTEX). *Bull. Amer. Meteorol. Soc.*, **78,** 1917–1940
Keyser, D., Reeder, M. J. and Reed, R. J.	1988	A generalization of Petterssen's frontogenesis function and its relation to the forcing of vertical motion. *Mon. Weather Rev.*, **116,** 762–780
Keyser, D., Schmidt, B. D. and Duffy, D. G.	1989	A technique for representing three-dimensional vertical circulations in baroclinic disturbances. *Mon. Weather Rev.*, **117,** 2463–2494
Loughe, A. F., Lai, C.-C. and Keyser, D.	1995	A technique for representing three-dimensional ageostrophic circulations in baroclinic disturbances on limited-area domains. *Mon. Weather Rev.*, **123,** 1476–1504
Malardel, S., Joly, A., Courbet, F. and Courtier, P.	1993	Nonlinear evolution of ordinary frontal waves induced by low-level potential vorticity anomalies. *Q. J. R. Meteorol. Soc.*, **119,** 681–713
McCallum E. and Grahame, N. S.	1993	The Braer storm—10 January 1993. *Weather*, **48,** 103–109
Nielsen, N. W.	1994	The 915-hPa cyclone of 10 January 1993. Pp. 301–306 in *The life cycle of extratropical cyclones.* Eds. S. Gronas and M. A. Shapiro, Bergen, Norway
Renfrew, I. A.	1995	'The development of secondary frontal cyclones'. Ph. D. Thesis, University of Reading

Renfrew, I. A., Thorpe, A. J. and Bishop, C. 1997 The role of environmental flow in the development of secondary frontal cyclones. *Q. J. R. Meteorol. Soc.*, **123**, 1653–1676

Schar, C. and Davies, H. C. 1990 An instability of mature cold fronts. *J. Atmos. Sci.*, **47**, 929–950

Thorncroft, C. D. and Hoskins, B. J. 1990 Frontal cyclogenesis. *J. Atmos. Sci.*, **47**, 2317–2336

Thorpe, A. J. 1994 'Dynamics of mesoscale sub-structure at fronts'. Pp. 220–228 in Life Cycles of Extra-Tropical Cyclones (vol I). Proceedings of the International Symposium, Bergen, Norway

Thorpe, A. and Emanuel, K. A. 1985 Frontogenesis in the presence of small stability to slantwise convection. *J. Atmos. Sci.*, **42**, 1809–1824

Vautard, R., Legras, B. and Déqué, B. 1988 On the source of midlatitude low-frequency variability. Part I: A statistical approach to persistance. *J. Atmos. Sci.*, **45**, 2811–2843